RSC Advances

PAPER

View Article Online
View Journal | View Issue

Cite this: *RSC Adv.*, 2025, **15**, 41340

Cycloartane-type saponins from *Curculigo orchioides* and their anti-inflammatory activity

Le Thanh Huong,[a] Vu Duong Bach,[a] Pham The Hai,[a] Vu Mai Thao,[b] Nguyen Xuan Nhiem[bc] and Nguyen Hai Dang *[a]

Received 7th July 2025
Accepted 18th October 2025

DOI: 10.1039/d5ra04849d

rsc.li/rsc-advances

Curculigo orchioides is a traditional medicinal plant used in Asia for treating inflammation and related ailments. In this study, nine compounds were isolated, including six novel cycloartane-type saponins, namely curculigosaponins P–U (**1–6**) and three known compounds. Among the six new compounds, compound **1** exhibited moderate inhibition of NO production (IC_{50} = 37.21 μM) in LPS-stimulated RAW 264.7 macrophages. It also suppressed the expression of TNF-α and IL-6, and downregulated iNOS and COX-2 protein levels, confirming its anti-inflammatory activity. Molecular docking analysis revealed favorable binding interactions of compound **1** with key inflammatory targets (iNOS, IL-6, TNF-α, and COX-2), supporting its proposed mechanism of action. These results suggest that compound **1** (curculigosaponins P) is a promising anti-inflammatory lead compound from *C. orchioides* and deserves further investigation.

Introduction

Inflammation is a complex biological response to harmful stimuli such as pathogens, damaged cells, or irritants. While acute inflammation is crucial in protecting the body and promoting tissue repair, chronic inflammation is associated with various serious diseases, including cancer, cardiovascular diseases, diabetes, and autoimmune disorders.[1] Currently, nonsteroidal anti-inflammatory drugs (NSAIDs) and corticosteroids are widely used for inflammation treatment. Still, their long-term use can cause severe side effects, including gastric ulcers, immune suppression, and liver damage.[2] Therefore, the search for more effective and safer anti-inflammatory agents, particularly from natural sources, has become an important research direction.[3]

Curculigo orchioides Gaertn., a plant belonging to the Hypoxidaceae family, is widely distributed in tropical and subtropical regions, including Vietnam, China, and India.[4] In traditional medicine, its rhizomes have been used to treat arthritis, asthma, and immune-related disorders.[4,5] Phytochemical studies have identified flavonoids, phenolic glycosides,[6] and cycloartane saponins,[7,8] which exhibit promising pharmacological activities such as antioxidant, immunomodulatory, and neuroprotective effects.[5,9] Among these, extracts from *C. orchioides* have been reported to exhibit potent anti-inflammatory effects by inhibiting of pro-inflammatory cytokines and oxidative stress.[10] However, there is no report on the anti-inflammatory potential of compounds from *C. orchioides*.

As part of our ongoing investigation into bioactive anti-inflammatories from medicinal plants in Vietnam, the methanol extract of *C. orchioides* roots was found to exhibit significant anti-inflammatory activity. Phytochemical analysis led to the isolation of six new cycloartane-type saponins and three known compounds. In this study, we report on the isolation, structural elucidation, and *in vitro* anti-inflammatory evaluation of these compounds using appropriate cellular and computational models.

Materials and methods

General experimental procedures

NMR spectra were recorded on a Bruker 600 MHz spectrometer. HR-ESI-MS spectra were obtained using a Waters ACQUITY UPLC system connected to a Xevo G2-XS QTOF at the Korea Basic Science Institute (KBSI, Metropolitan Seoul Center). Column chromatography (CC) was performed on silica gel (Kieselgel 60, 70–230 mesh and 230–400 mesh, Merck) or RP-18 gel (30–50 μm, Fuji Silysia Chemical Ltd.). For thin layer chromatography (TLC), pre-coated silica gel 60 F_{254} (0.25 mm, Merck) and RP-18 $F_{254}S$ (0.25 mm, Merck) plates were used. The HPLC system was an Agilent HPLC 1100 (General condition: J'sphere H-80 column: 250 mm length × 20 mm ID and a flow rate of 3 mL min^{-1}), detector DAD. Spots were visualized by spraying with 10% aqueous H_2SO_4, followed by heating.

Plant materials. The roots of *Curculigo orchioides* Gaertn. were collected in Lang Son province, Vietnam in June 2024, and

[a]*University of Science and Technology of Hanoi, Vietnam Academy of Science and Technology (VAST), 18 Hoang Quoc Viet, Hanoi, Vietnam. E-mail: nguyen-hai.dang@usth.edu.vn*

[b]*Institute of Chemistry, VAST, 18 Hoang Quoc Viet, Hanoi, Vietnam*

[c]*Graduate University of Science and Technology, VAST, 18 Hoang Quoc Viet, Hanoi, Vietnam*

identified by Prof. Ninh Khac Ban, Institute of Chemistry, VAST. A voucher specimen (USTH-CO) was deposited at the University of Science and Technology of Hanoi, VAST.

Extraction and isolation. The air-dried roots of *Curculigo orchioides* Gaertn (3.0 kg) were extracted twice with methanol (MeOH, 15 L each, 2 h, 45 °C), and the combined extracts were concentrated under reduced pressure to afford a MeOH crude extract (300 g). This extract was dissolved in water and subsequently partitioned with *n*-hexane and ethyl acetate (EtOAc) to yield three fractions: *n*-hexane (RCO1, 25 g), EtOAc (RCO2, 20.4 g), and aqueous (RCO3) layer.

The aqueous fraction (RCO3) was subjected to Diaion HP-20 column chromatography (CC) using a gradient of 50 and 75 MeOH in water and then MeOH, affording three fractions: RCO3A (37.0 g), RCO3B (12.0 g), and RCO3C (1.5 g). RCO3A was chromatographed on a silica gel CC, eluted with CH_2Cl_2 : MeOH (20 : 1 → 2 : 1, v/v), yielding two fractions, RCO3A1 and RCO3A2. The RCO3A2 fraction was subjected to a silica gel CC using CH_2Cl_2 : acetone : H_2O (1 : 2.5 : 0.15, v/v/v), resulting in three subfractions (RCO3A2A–RCO3A2C). Among them, RCO3A2B was purified on an RP-18 CC and eluted with acetone : H_2O (1 : 4, v/v), to afford two fractions, RCO3A2B1 and RCO3A2B2. RCO3A2B1 was purified on a sephadex LH-20 CC (90% MeOH in water), then on an HPLC eluting with 18% acetonitrile (ACN) in water to yield compound **8** (14 mg, t_R = 29.8 min). RCO3B was subjected to a silica gel CC eluting with CH_2Cl_2 : MeOH (20 : 1, 10 : 1, 5 : 1, 2 : 1, v/v), giving fractions, RCO3B1–RCO3B4. RCO3B2 was further chromatographed on a silica gel CC with CH_2Cl_2 : acetone : H_2O (1 : 1.5 : 0.1, v/v/v), followed by an RP-18 CC (MeOH : H_2O, 1 : 1, v/v) affording RCO3B2A–RCO3B2C. RCO3B2A was purified on an HPLC eluting with 18% ACN in water to yield **7** (14.5 mg, t_R = 29.3 min). RCO3B3 was chromatographed on a silica gel CC using CH_2Cl_2 : acetone : H_2O (1 : 2 : 0.15, v/v/v) to give RCO3B3A–RCO3B3C. RCO3B3B was chromatographed on an RP-18 CC (MeOH : H_2O, 1 : 1, v/v) then purified on an HPLC eluting with 25% ACN in water to yield **9** (6.0 mg, t_R = 29.3 min). RCO3B3C was chromatographed on an RP-18 CC (MeOH : H_2O, 1 : 2, v/v) affording RCO3B3C1 and RCO3B3C2. RCO3B3C1 was then purified on an HPLC eluting with 30% ACN in water to yield compounds **1** (6.3 mg, t_R = 32.4 min) and **5** (14.0 mg, t_R = 27.6). Finally, RCO3B3C2 was purified on an HPLC eluting with 30% ACN in water to yield compounds **2** (7.0 mg, t_R = 37.5 min), **3** (15.0 mg, t_R = 33.9 min), **4** (7.5 mg, t_R = 43.4 min), and **6** (7.5 mg, t_R = 52.7 min).

Spectroscopic data

*Curculigosaponin P (**1**).* White amorphous powder; $[\alpha]_D^{25}$ +20.7 (*c* 0.1, MeOH); $C_{41}H_{66}O_{13}$, HRESIMS *m*/*z*: 767.4544 (calcd for $[C_{41}H_{67}O_{13}]^+$, 767.4576); for ^{1}H (CD_3OD, 600 MHz) and ^{13}C NMR (CD_3OD, 150 MHz) spectroscopic data, see Table S2.

*Curculigosaponin Q (**2**).* White amorphous powder; $[\alpha]_D^{25}$ +15.0 (*c* 0.1, MeOH); $C_{41}H_{66}O_{13}$, HRESIMS *m*/*z*: 767.4532 (calcd for $[C_{41}H_{67}O_{13}]^+$, 767.4576); for ^{1}H (CD_3OD, 600 MHz) and ^{13}C NMR (CD_3OD, 150 MHz) spectroscopic data, see Table S2.

*Curculigosaponin R (**3**).* White amorphous powder; $[\alpha]_D^{25}$ +35.2 (*c* 0.1, MeOH); $C_{41}H_{66}O_{13}$, HRESIMS *m*/*z*: 767.4547 (calcd for $[C_{41}H_{67}O_{13}]^+$, 767.4576); for ^{1}H (CD_3OD, 600 MHz) and ^{13}C NMR (CD_3OD, 150 MHz) spectroscopic data, see Table S2.

*Curculigosaponin S (**4**).* White amorphous powder; $[\alpha]_D^{25}$ +42.0 (*c* 0.1, MeOH); $C_{41}H_{66}O_{13}$, HRESIMS *m*/*z*: 767.4545 (calcd for $[C_{41}H_{67}O_{13}]^+$, 767.4576); for ^{1}H (CD_3OD, 600 MHz) and ^{13}C NMR (CD_3OD, 150 MHz) spectroscopic data, see Table S3.

*Curculigosaponin T (**5**).* White, amorphous powder; $[\alpha]_D^{25}$ +8.4 (*c* 0.1, MeOH); $C_{41}H_{66}O_{14}$, HRESIMS *m*/*z*: 783.4497 (calcd for $[C_{41}H_{67}O_{14}]^+$, 783.4525); for ^{1}H (CD_3OD, 600 MHz) and ^{13}C NMR (CD_3OD, 150 MHz) spectroscopic data, see Table S3.

*Curculigosaponin U (**6**).* White amorphous powder; $[\alpha]_D^{25}$ +48.6 (*c* 0.1, MeOH); $C_{42}H_{68}O_{14}$, HRESIMS *m*/*z*: 797.4645 (calcd for $[C_{42}H_{69}O_{14}]^+$, 797.4682); for ^{1}H (CD_3OD, 600 MHz) and ^{13}C NMR (CD_3OD, 150 MHz) spectroscopic data, see Table S3.

Acid hydrolysis and sugar analysis. Each compound (**1–6**, 2.0 mg) was separately dissolved in 1.0 N HCl (dioxane–H_2O, 1 : 1, v/v, 1.0 mL) and heated to 80 °C in a water bath for 3 h. Acidic solution was neutralized with Ag_2CO_3 with the solvent thoroughly removed under a N_2 stream overnight. After extraction with $CHCl_3$, the aqueous layer was concentrated to dryness using N_2. The residue was dissolved in dry pyridine (0.1 mL), followed by addition of L-cysteine methyl ester hydrochloride in pyridine (0.06 M, 0.1 mL). The reaction mixture was heated at 60 °C for 2 h. Trimethylsilylimidazole solution (0.1 mL) was then added, followed by heating at 60 °C for 1.5 h. The dried product was partitioned with *n*-hexane and H_2O (0.1 mL each), and the organic layer was analyzed by gas chromatography (GC): column DB-5 (0.32 mm ID × 30 m length), detector FID, column temp 210 °C, injector temp 270 °C, detector temp 300 °C, carrier gas He (2 mL min^{-1}). Under these conditions, the standard sugars gave peaks at t_R (min) 14.11 and 14.26 for D- and L-glucose, 9.82 and 15.24 for D- and L-arabinose, 8.21 and 8.66 for D- and L-xylose, and 4.50 for L-rhamnose, respectively. Peaks at t_R (min) 14.11 and 15.24 of D-glucose and L-arabinose for **1** and **3**; 14.11 and 8.21 of D-glucose and D-xylose for **2**, **4**, and **5**; 14.11 and 4.50 of D-glucose and L-rhamnose for **6** were observed, respectively.

Anti-inflammatory assay

Cell culture. RAW 264.7 macrophages were purchased American Type Culture Collection (ATCC, Virginia, USA) and grown in Dulbecco's Modified Essential Medium (DMEM, Gibco, USA) medium supplemented with 10% fetal bovine serum (FBS) and 1% penicillin–streptomycin solution (Gibco, USA) in a humidified atmosphere containing 5% CO_2 at 37 °C.

Cell viability assay. Cell viability was determined by a 3-(4,5-dimethylthiazole-2-yl)-2,5-diphenyl-tetrazolium bromide (MTT) assay. Briefly, RAW 264.7 cells at a density of 5 × 10^4 cells per well were seeded into 96-well plates and cultured in 37 °C, 5% CO_2 incubator for 24 h. The cells were treated with samples at various concentrations. After 24 h, the cells were incubated with 20 μL of MTT solution (5 mg mL^{-1}) for an additional 3–4 h. After removing the supernatant, the formazan crystals that had formed were dissolved by the addition of 200 μL dimethyl sulfoxide (DMSO) and agitation for 10 min at room

temperature. The formation of formazan was measured by reading absorbance at a wavelength of 570 nm in a spectrometer (Biotek, USA).

Measurement of NO production. RAW 264.7 cells were seeded in a 96-well culture plate at a density of 5×10^4 cells per well in an incubator at 37 °C, 5% CO_2. After 24 h, cells were pretreated with various concentrations of the tested samples for 30 min and then incubated with 1 μg mL^{-1} LPS for 24 h. NO production in the culture supernatant was determined by using Griess reagent and incubating in the dark at room temperature for 10 min. The concentration of NO was measured in a spectrometer at 540 nm.

Measurement of IL-6 and TNF-α production. RAW 264.7 cells were seeded at a density of 2×10^5 cells per well in a 24-well plate overnight. The cells were pre-incubated for 30 min with various concentrations of the tested samples and stimulated for 24 h with 1 μg mL^{-1} LPS. The cell culture supernatants were collected and centrifuged at 1000*g* for 15 min to remove the particulate matter. IL-6 (thermo-scientific) and TNF-α (Elabscience) were determined using an enzyme immunoassay (EIA) kit according to the manufacturer's instructions.

Western blotting. RAW 264.7 cells were seeded in six-well plates at a density of 2×10^5 cells per well in an incubator at 37 °C, 5% CO_2 for 24 h. Cells were then treated with various concentrations of the tested samples for 30 min, followed by subsequent incubation with LPS at 1 μg mL^{-1} for 24 h. Cells were harvested and washed twice with PBS. The cell solution was centrifuged at 5000*g* for 3 min. The pellet was resuspended in lysis buffer and incubated for 30 min on ice. The mixture was centrifuged at 10 000*g* for 10 min to collect the supernatant. Proteins in the supernatant were quantified using a BSA assay kit (Thermo Fisher Scientific Inc.). Quantified protein was mixed with 4× sample buffer and incubated for 10 min at 100 °C. The protein samples were separated by 10% or 12% SDS–PAGE and transferred onto nitrocellulose membranes. The membrane was then blocked with 5% skim milk for 2 h, followed by incubating with the primary antibodies overnight at 4 °C. After that, the membrane was washed 3 times for 10 min with phosphate-buffered saline Tween-20 (PBST) and then incubated with secondary antibodies for 2 h at room temperature. After washing 3 times for 10 min with PBST buffer, the proteins were visualized using Pierce™ Enhanced chemiluminescent (ECL) western blotting substrate (Thermo Fisher Scientific) and imaged using the Azure C300 system.

Statistical analysis. Experiments were repeated at least three times, and all data were expressed as means ± SD. Statistical significance was evaluated using *t*-tests and one-way ANOVAs, where $p < 0.05$ was considered significant.

Docking studies

The 3D structures of four target enzymes were retrieved from the RCSB Protein Data Bank (**https://www.rcsb.org**), including iNOS (PDB ID: 3E7G),[11] IL-6 (PDB ID: 1ALU),[12] TNF-α (7JRA),[13] and COX-2 (5KIR).[14] All the ligand structures were constructed and optimized using MOE 2015.10.[15] Similar to the previous studies, both ligands and protein structures were prepared in MOE, including hydrogen addition, energy minimization, and force field assignment (AMBER99).[16,17] Binding sites were identified using MOE's Site Finder tool and fixed using dummies for docking. Protocol validation was performed by removing and redocking co-crystallized ligands into their respective protein targets. The binding energies (ΔG, kcal mol^{-1}) were calculated using London and GBVI/WSA scoring functions. The Root Mean Square Deviation (RMSD) between the original and redocked poses was calculated to confirm docking reliability. A RMSD value below 2.0 Å was considered acceptable for a successful protocol.[18] Subsequently, the selected natural compounds were docked into the enzyme binding sites using default docking parameters implemented in MOE. For each ligand, 10 poses were generated, and the best pose was selected based on binding energy and interaction profiles. Docking results were visualized using Chimera X and Discovery Studio 2024 to examine the physicochemical nature of the binding pockets and binding interactions with the key residues.[19]

Result and discussion

Extraction and isolation

Six new compounds, curculigosaponins P–T (**1–6**) (Fig. 1) and three known compounds, tricalysioside U (**7**),[20] zingiberoside B (**8**),[21] and apigenin 7-*O*-β-D-glucopyranoside (**9**)[22] were isolated and identified. Their chemical structures were elucidated by spectroscopic and chemical methods and comparison with reported data in the literature.

Compound **1** was obtained as an amorphous powder, and its molecular formula was established to be $C_{41}H_{66}O_{13}$ by HR-ESI-MS data at *m*/*z* 767.4544 (calcd for $[C_{41}H_{67}O_{13}]^+$, 767.4576). The ^{1}H-NMR spectrum exhibited one olefinic proton at δ_H 5.29 (d, J = 8.4 Hz), two protons of the cyclopropane ring at δ_H 0.46 (d, J = 4.2 Hz) and 0.57 (d, J = 4.2 Hz), six tertiary methyl groups at δ_H 0.91, 1.01, 1.07, 1.14, 1.72, and 1.74 (each 3H, s) characteristic of a cycloartane triterpene-type aglycone, two anomeric protons at δ_H 4.18 (1H, d, J = 6.6 Hz) and 4.35 (1H, d, J = 7.8 Hz), suggesting the presence of two sugar moieties. The ^{13}C-NMR and HSQC spectra of **1** exhibited signals of 41 carbons, including two olefinic carbons at δ_C 127.9 and 136.1, five quaternary carbons at δ_C 20.9, 27.2, 42.0, 47.7, and 50.6, seventeen methine carbons at δ_C 38.0, 48.7, 49.0, 50.3, 69.5, 71.7, 72.8, 73.1, 74.2, 75.7, 76.2, 77.7, 78.3, 83.9, 90.3, 106.7, and 107.0, and eleven methylene carbons at δ_C 22.2, 27.5, 30.3, 31.1, 33.3, 39.6, 40.4, 50.5, 62.8, 66.8 and 72.2, along with six methyl carbons at δ_C 15.5, 18.1, 19.7, 21.9, 25.9, and 26.0. Analysis of ^{1}H- and ^{13}C-NMR data indicated the structure of **1** was similar to that of (23*R*)-21,23-epoxy-5α-cycloart-24-en-3β-ol[23] except for additions of saccharide moieties at C-3 and C-16 and a hydroxy group at C-12. The HMBC correlations between H-28 (δ_H 0.91)/H-29 (δ_H 1.07) and C-3 (δ_C 90.3)/C-4 (δ_C 42.0)/C-5 (δ_C 49.0) suggested the presence of an oxygenated functional group at C-3. The multiplicity of H-3 [δ_H 3.27 (dd, J = 4.2, 11.4 Hz)] indicated the *axial* orientation of H-3, which was further supported by NOESY correlation between H-3 (δ_H 3.27) and H-29 (δ_H 1.07). The HMBC correlations between H-26 (δ_H 1.74)/H-27 (δ_H 1.72) and C-24 (δ_C

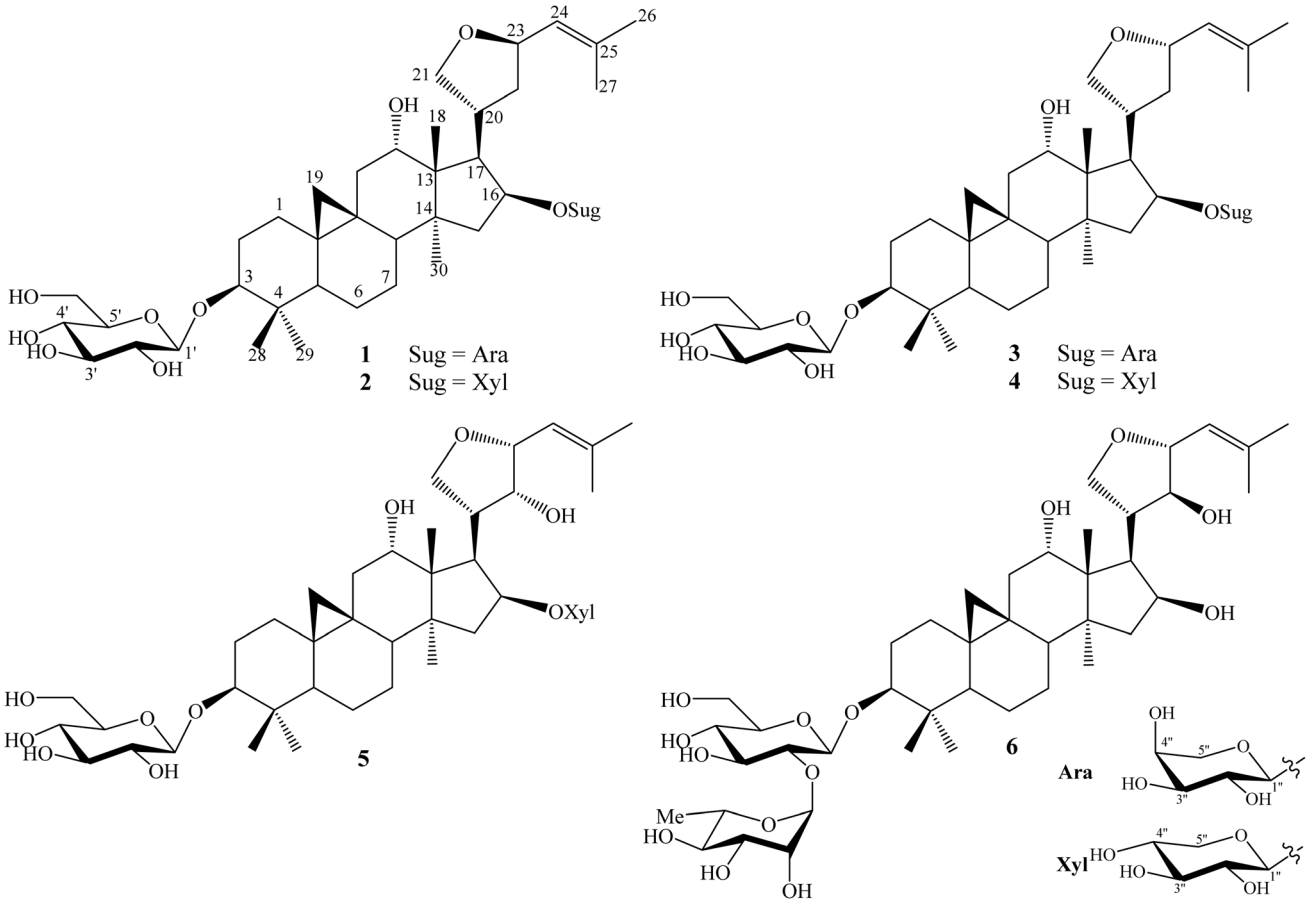

Fig. 1 Chemical structures of compounds of **1–6**.

127.9)/C-25 (δ_C 136.1) confirmed the position of a double bond at C-24/C-25. The HMBC correlations between H-18 (δ_H 1.14) and C-12 (δ_C 73.1)/C-13 (δ_C 47.7)/C-14 (δ_C 50.6)/C-17 (δ_C 48.7) indicated the position of the hydroxy group at C-12. Furthermore, the α configuration of the hydroxy group at C-12 was confirmed by NOESY correlation of H-12 (δ_H 3.63)/H-18 (δ_H 1.14). The HMBC correlations between H-21 (δ_H 3.73 and 4.00) and C-20 (δ_C 38.0)/C-22 (δ_C 39.6)/C-23 (δ_C 76.2) along with COSY correlations between H-21 (δ_H 3.73 and 4.00)/H-20 (δ_H 2.70)/H-22 (δ_H 1.80 and 2.18)/H-23 (δ_H 4.66) indicated the presence of an epoxy group at C-21/C-23. The α configuration of H-23 was confirmed by NOESY correlations between H_β-21 (δ_H 4.00) and H-20 (δ_H 2.70); H_α-21 (δ_H 3.73) and H-23 (δ_H 4.66). The HMBC correlations between H-15 (δ_H 1.74 and 2.03) and C-16 (δ_C 83.9) as well as COSY correlations of H-15 (δ_H 1.74 and 2.03)/H-16 (δ_H 4.14)/H-17 (δ_H 2.59) indicated the presence of the oxygenated group at C-16. In addition, the α configuration of H-16 was proved by NOE observation between H-16 (δ_H 4.14) and H-17 (δ_H 2.59). The sugar moieties were determined by acid hydrolysis followed by TMS derivative analysis by GC method, confirming the presence of D-glucose and L-arabinose. Additionally, the large coupling constants of glc H-1′ and glc H-2′ ($J = 7.8$ Hz) and ara H-1″ and ara H-2″ ($J = 6.6$ Hz), confirmed the presence of β-D-glucopyranosyl and α-L-arabinopyranosyl moieties. The positions of β-D-glucopyranosyl and α-L-arabinopyranosyl moieties at C-3 and C-16, respectively were established by HMBC correlations between glc H-1′ (δ_H 4.35) and C-3 (δ_C 90.3), and between ara H-1″ (δ_H 4.18) and C-16 (δ_C 83.9). Based on the above evidence and chemical analysis, the structure of **1** was elucidated, a new compound named curculigosaponin P.

Compound **2** was isolated as a white amorphous powder. Its molecular formula was determined to be $C_{41}H_{66}O_{13}$ on the basis of HR-ESI-MS, which exhibited a pseudomolecular ion peak at m/z 767.4532 $[M + H]^+$ (calcd for $[C_{41}H_{67}O_{13}]^+$, 767.4576). The ^{1}H-NMR spectrum of **2** showed a closely related pattern to that of **1**, with characteristic resonances for a cycloartane-type triterpene, including an olefinic proton at δ_H 5.28 (1H, d, $J = 8.4$ Hz) and two protons of cyclopropane ring at δ_H 0.45 and 0.57 (each 1H, d, $J = 4.2$ Hz). Signals of six tertiary methyl groups were also observed at δ_H 0.91, 1.00, 1.07, 1.13, 1.72, and 1.73 (each 3H, s). The sugar region revealed signals of two anomeric protons at δ_H 4.16 (1H, d, $J = 7.8$ Hz) and 4.35 (1H, d, $J = 7.8$ Hz), suggesting the presence of two monosaccharides. The ^{13}C-NMR and HSQC spectra displayed signals of 41 carbons, including 2 olefinic carbons, 5 quaternaries, 17 methines, 11 methylenes, and 6 methyl carbons. Analysis of ^{1}H- and ^{13}C-NMR data indicated the structure of **2** was similar to that of **1** except for different sugar moiety at C-16. The sugar moieties were determined D-glucose and D-xylose using acid hydrolysis (identified as TMS derivative by GC method). A deshielded methine carbon

at δ_C 90.3 (C-3) was assigned as the site of glucosylation, supported by HMBC correlation between glc H-1′ (δ_H 4.35) and C-3 (δ_C 90.3). Similarly, the xylopyranosyl moiety was linked to C-16, confirming by HMBC correlation between xyl H-1″ (δ_H 4.16) and C-16 (δ_C 83.9) and between H-15 (δ_H 1.66 and 2.02) and C-16 (δ_C 83.9) as well as COSY correlations of H-15 (δ_H 1.66 and 2.02)/H-16 (δ_H 4.14)/H-17 (δ_H 2.58). The NOESY correlation between H-16 (δ_H 4.14) and H-17 (δ_H 2.58) suggested the hydroxyl group at C-16 to be α-oriented. The α-orientation of the hydroxyl group at C-12 remained unchanged compared to **1**, as evidenced by NOESY correlation between H-12 (δ_H 3.63) and H-18 (δ_H 1.13). The double bond was located at C-24/C-25 confirming by HMBC correlations from H-26 (δ_H 1.73) and H-27 (δ_H 1.72) to C-24 (δ_C 127.8) and C-25 (δ_C 136.3). Additionally, the presence of an epoxy ring between at C-21/C-23 was suggested by HMBC correlations from H-20 (δ_H 2.71) to C-22 (δ_C 39.5)/C-23 (δ_C 76.3), from H-23 (δ_H 4.65) to C-21 (δ_C 72.2)/C-22 (δ_C 39.5) as well as COSY correlations of H-21 (δ_H 3.72 and 4.00)/H-20 (δ_H 2.71)/H-22 (δ_H 1.80 and 2.20)/H-23 (δ_H 4.65). The large coupling constants (J = 7.8 Hz for both glc H-1′/H-2′ and ara H-1″/H-2″) indicated that both monosaccharides were β-pyranose configuration. Accordingly, compound **2** was identified, a new compound named curculigosaponin Q.

Compound **3** was also isolated as a white amorphous powder, and its molecular formula $C_{41}H_{66}O_{13}$ was confirmed by HR-ESI-MS, which exhibited a pseudomolecular ion peak at m/z 767.4547 $[M + H]^+$ (calcd for $[C_{41}H_{67}O_{13}]^+$, 767.4576). The ^{1}H-NMR spectrum revealed signal pattern indicative of a cycloartane-type triterpene backbone, including one olefinic proton at δ_H 5.22 (d, J = 8.4 Hz), two protons of cyclopropane ring at δ_H 0.45 and 0.57 (each d, J = 4.2 Hz), and six tertiary methyl at δ_H 0.91, 1.00, 1.07, 1.13, 1.70, and 1.73 (each 3H, s), two monosaccharide units with the presence of two anomeric protons at δ_H 4.16 (d, J = 6.6 Hz) and 4.35 (d, J = 7.8 Hz). The ^{13}C-NMR and HSQC spectra of **3** displayed signals of 41 carbons. The NMR data of **3** were similar to those of **1**, indicated they have similar constitutional structure except for the difference of ^{13}C-NMR chemical shifts at C-22 and C-23 [δ_C 39.6 (C-22) and 76.2 (C-23)] for compound **1**; δ_C 41.0 (C-22) and 77.0 (C-23) for compound **3**. These findings suggested the possible different stereochemistry center at C-23. The β-orientation of H-23 was further confirmed by NOESY correlations between H-20 (δ_H 2.72) and H_β-21 (δ_H 3.94)/H-23 (δ_H 4.66) and between H-18 (δ_H 1.13) and H_β-21 (δ_H 3.94)/H-20 (δ_H 2.72). Acid hydrolysis gave glucose and arabinose (identified as TMS derivatives by GC method). Moreover, the HMBC correlation from glc H-1′ (δ_H 4.35) to C-3 (δ_C 90.3) confirmed the position of the β-D-glucopyranosyl moiety at C-3, while the second monosaccharide, α-L-arabinopyranosyl moiety was established at C-16 by the HMBC correlation from H-1″ (δ_H 4.16) to C-16 (δ_C 83.9). As in previous compounds, the presence of a double bond at C-24/C-25 was supported by HMBC cross-peaks from H-26 (δ_H 1.74)/H-27 to C-24 (δ_C 127.7)/C-25 (δ_C 136.3). Based on these findings, the structure of new compound **3** was determined and named curculigosaponin R.

Compound **4** was isolated as a white amorphous powder and assigned the molecular formula $C_{41}H_{66}O_{13}$ based on HR-ESI-MS data (m/z at 767.4545 $[M + H]^+$, calcd for $[C_{41}H_{67}O_{13}]^+$, 767.4576). The ^{1}H-NMR spectrum of **4** displayed typical signals of a cycloartane-type triterpene saponin, including an olefinic proton at δ_H 5.22 (d, J = 8.4 Hz), while two distinct doublets at δ_H 0.46 and 0.57 (each 1H, d, J = 4.2 Hz) were ascribed to protons of a cyclopropane ring. Six tertiary methyl groups were observed at δ_H 0.91, 0.99, 1.07, 1.13, 1.70, and 1.74. Two anomeric proton signals at δ_H 4.17 (d, J = 7.2 Hz) and 4.35 (d, J = 7.8 Hz) indicated the presence of two sugar moieties. The ^{13}C-NMR and HSQC spectra of **4** showed signals of 41 carbons. The NMR data of **4** were found to be similar to those of **3** except for the difference of monosaccharide moiety at C-16. Sugar components, glucose and xylose moieties were identified under TMS derivatives by GC method. The positions of glucopyranosyl and xylopyranosyl moieties at C-3 and C-16, respectively, were determined by HMBC correlations between glc H-1′ (δ_H 4.35) and C-3 (δ_C 90.3) and between xyl H-1 (δ_H 4.18) and C-16 (δ_C 83.9). The HMBC correlation between H-18 (δ_H 1.13) and C-12 (δ_C 73.0)/C-13 (δ_C 47.6)/C-14 (δ_C 50.6)/C-17 (δ_C 48.5) established the presence and location of a hydroxyl group at C-12, whose β-orientation is corroborated by NOESY interaction between H-12 (δ_H 3.60) and H-18 (δ_H 1.13). Consequently, the new structure of **4** was named curculigosaponin S.

Compound **5** was obtained as a white amorphous powder and assigned the molecular formula $C_{41}H_{66}O_{14}$ based on HR-ESI-MS data, which displayed a pseudomolecular ion peak at m/z 783.4497 (calcd for $[C_{41}H_{67}O_{14}]^+$, 783.4525). The ^{1}H and ^{13}C-NMR spectral data of **5** were similar to those of **4** except for the addition of a hydroxy group at C-22 of the 21,23-epoxy ring. The position of a hydroxyl group at C-22 was proved by HMBC correlations from H-17 (δ_H 2.69)/H-21 (δ_H 3.88 and 4.09)/H-23 (δ_H 4.38)/H-24 (δ_H 5.33) to C-22 (δ_C 84.0). The α-configuration of H-22 was proven by NOESY correlations between H-22 (δ_H 3.83) and H-20 (δ_H 2.69)/H_β-23 (δ_H 4.38) as well as a small coupling constant of H-22 and H-23, J = 4.2 Hz. The HMBC correlations between the glc H-1′ (δ_H 4.35) and C-3 (δ_C 90.2) and between xyl H-1″ (δ_H 4.24) and C-16 (δ_C 84.1) confirmed the glucosylation at C-3 and xylosylation at C-16. Consequently, the new structure of **5** was elucidated and named curculigosaponin T.

Curculigosaponin U (**6**) was obtained as a white amorphous powder. Its molecular formula was established to be $C_{42}H_{68}O_{14}$ by HR-ESI-MS, which exhibited a pseudomolecular ion peak at m/z 797.4645 $[M + H]^+$ (calcd for $C_{42}H_{69}O_{14}^+$, 797.4682), corresponding to 12 degrees of unsaturation. The ^{1}H-NMR spectrum displayed typical signals for a cycloartane-type triterpene aglycone, including an olefinic proton at δ_H 5.22 (d, J = 9.0 Hz), two protons of the cyclopropane ring at δ_H 0.46 and 0.59 (each d, J = 4.2 Hz), and six methyl singlets ranging from δ_H 0.92 to 1.79. The ^{13}C-NMR and HSQC spectra of **6** showed the presence of 42 carbons, including 6 quaternaries, 20 methines, 9 methylenes, and 7 methyls. Analysis of ^{1}H- and ^{13}C-NMR data indicated the structure of **6** was similar to **5** except for the change position of sugar moiety from C-16 of cycloartane to C-2 of monosaccharide. The position of a hydroxyl group at C-22 was indicated by HMBC correlations from H-17 (δ_H 2.55)/H-21 (δ_H 4.09 and 4.10)/H-23 (δ_H 4.35)/H-24 (δ_H 5.22) to C-22 (δ_C 83.0). The α-

configuration of H-22 was proven by NOESY correlation between H-22 (δ_H 3.83) and H-17 (δ_H 2.55) as well as a large coupling constant of H-22 and H-23, $J = 7.2$ Hz. Acid hydrolysis of **6** followed by derivatization and GC analysis of the TMS derivatives, confirmed the presence of D-glucose and L-rhamnose. The multiplicity of glucose anomeric proton glc H-1′ (δ_H 4.44, d, $J = 7.2$ Hz) indicated β-configuration, while the rha H-1″ (δ_H 5.40, d, $J = 1.2$ Hz) indicated an α-L-rhamnopyranosyl unit. The HMBC correlations between rha H-1″ (δ_H 5.40) and glc C-2′ (δ_C 79.0) and between glc H-1′ (δ_H 4.44) and glc C-3 (δ_C 89.6) suggested sugar linkage as α-L-rhamnopyranosyl-(1→2)-*O*-β-D-glucopyranosyl and at C-3 of cycloartane aglycone. Based on the above evidence, the structure of **6** was elucidated.

Investigation of the NO inhibitory effect of curculigosaponins P–U on LPS-stimulated murine macrophage RAW 264.7 cells

Three known compounds—tricalysioside U (**7**), zingiberoside B (**8**), and apigenin 7-*O*-β-D-glucopyranoside (**9**) were isolated during the phytochemical evaluation of *Curculigo orchioides*. Among them, compound **9** has been reported for its anti-inflammatory and cytotoxic properties in many reports.[24–26] Our study focused instead on evaluating the six newly discovered compounds, for which no prior biological data existed, to explore their potential as novel bioactive agents. NO concentration assays were performed to estimate the anti-inflammatory effects of the six compounds. Concentrations of 30 μM and 100 μM were used for cell treatment for 24 h, with or without LPS (1 μg mL^{-1}) on RAW 264.7 macrophage cells. The effects of the compounds on cell viability were also examined. After screening, compounds **1**, **2**, **3**, **4**, and **6** showed NO inhibition properties. At a concentration of 100 μM, the curculigosaponins caused NO inhibition ranging from 69.98 to 95.05%. At the same time, these compounds were also non-cytotoxic with cell viability above 82% (SI Table S1).

The effective compounds were evaluated for IC_{50} values, the results are shown in Table 1.

Cardamonin was used as a positive control to evaluate the anti-inflammatory effects of LPS stimulation in RAW 264.7 cells as in our previous study.[27] Compared to cardamonin, compounds **3**, **4**, and **6** exhibited weaker NO inhibitory activity, with IC_{50} values of 89.68 and 58.28 μM, respectively (Table 1).

Compound **1** exhibited significant NO inhibitory activity, with an IC_{50} of 37.21 μM (Fig. 2). Based on this value and initial findings, **1** was selected for further investigation on the molecular mechanisms underlying its anti-inflammatory effects.

Table 1 The IC_{50} values for NO inhibition effect of curculigosaponins on RAW 264.7 cells

Compounds	The IC_{50} values[b] (μM)
1	37.21 ± 1.40
2	47.45 ± 1.93
3	91.39 ± 1.71
4	89.68 ± 2.41
6	58.28 ± 3.87
Cardamonin[a]	1.98 ± 0.05

[a] The positive control. [b] Experiments were performed in triplicate.

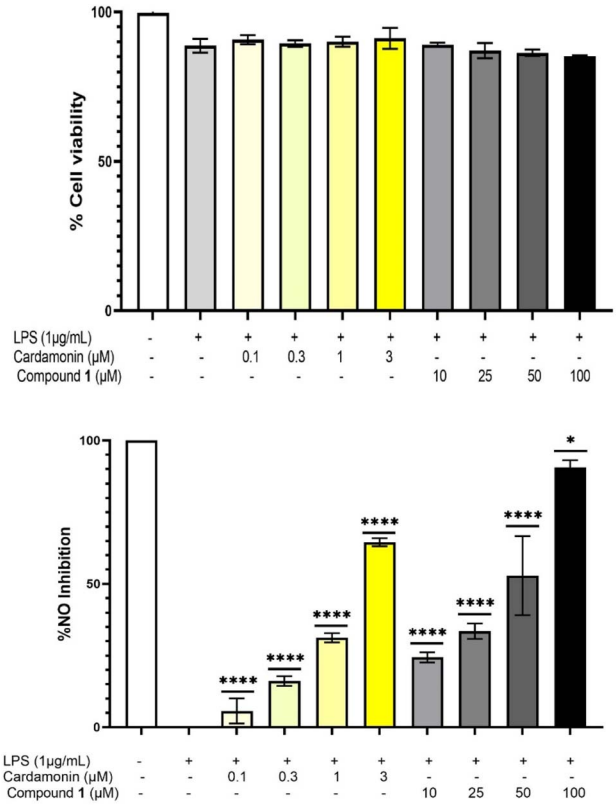

Fig. 2 Evaluation of cell viability and NO production of LPS-stimulated RAW 264.7 cells treated with compound **1**. Cells were pre-treated with various concentrations of compound **1** (10, 25, 50, and 100 μg mL^{-1}) for 30 minutes, followed by stimulation with LPS (1 μg mL^{-1}) for 24 hours. Cell viability was assessed using the MTT assay, with absorbance measured at 570. Nitric oxide levels were determined using the Griess assay, with absorbance measured at 540 nm. The data are expressed as mean ± SD ($n = 3$; *$p < 0.05$ ***$p < 0.001$, ****$p < 0.0001$, compared to LPS-treated controls).

Compound 1 inhibited LPS-induced TNF-α and IL-6 secretion in LPS-murine macrophage RAW 264.7 cells. TNF-α and IL-6 are key pro-inflammatory cytokines that play a vital role in immune response during inflammation. To assess their expression, ELISA was performed on RAW 264.7 cells. As shown in Fig. 2, LPS stimulation led to a significant increase in TNF-α and IL-6 levels. Notably, pretreatment with compound **1** (10–50–100 μM) markedly reduced the expression of both cytokines. These findings indicate that compound **1** effectively inhibits the production of inflammatory mediators TNF-α and IL-6 in LPS-stimulated RAW 264.7 cells (Fig. 3).

Compound 1 suppressed the LPS-stimulated expression of COX-2 and iNOS in murine macrophage RAW 264.7 cells. After 24 hours of treatment, the effects of **1** on iNOS and COX-2 protein expression in RAW 264.7 macrophages was analyzed using western blot. The results showed that LPS-stimulated RAW 264.7 cells had a significant increase in iNOS and COX-2 protein levels, consistent with the activation of pro-inflammatory signaling pathways, confirming the successful

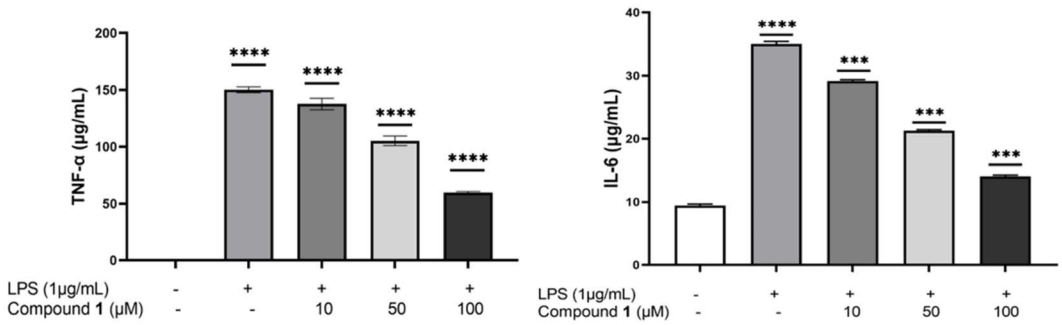

Fig. 3 Compound **1** inhibits LPS-induced TNF-α and IL-6 secretion in LPS-murine macrophage RAW 264.7 cells. Cells were pre-treated with different concentrations of **1** (10, 50, 100 μM) for 30 min, then stimulated with LPS (1 μg mL^{-1}) for 24 h. TNF-α and IL-6 levels in the supernatant were measured by ELISA. Each bar shows the mean ± SD of three independent experiments performed in triplicate (****$p < 0.0001$, ***$p < 0.001$ compared to LPS).

induction of inflammation in the LPS-treated cells, which provides a valid model for assessing the anti-inflammatory effects of compound **1**. Notably, treatment with compound **1** led to a substantial reduction in iNOS and COX-2 expression at all treated concentrations (Fig. 4). These findings demonstrate that compound **1** exerts an inhibitory effect on the expression of key pro-inflammatory mediators, COX-2 and iNOS.

Previous research has demonstrated that stimulation of RAW 264.7 macrophages with LPS typically leads to the increased phosphorylation and activation of ERK1/2, JNK, and p38 MAPKs,[28] which in turn activate NF-κB transcription pathway. After that, NF-κB enters the nucleus and promotes the production of inflammatory cytokines such as NO, PGE2, IL-6, and TNF-α (Fig. 5A). The elevated levels of NO and PGE2, two key pro-inflammatory mediators involved in cytotoxic and pro-apoptotic processes, are directly associated with the upregulation of iNOS and COX-2 expression. Our results demonstrated that compound **1** effectively inhibited the expression of inducible iNOS and COX-2, two key enzymes involved in the inflammatory response. In addition, compound **1** significantly suppressed the production of pro-inflammatory mediators IL-6 and TNF-α. These findings strongly indicate the anti-inflammatory potential of this compound. To date, there have been limited studies on the isolation and biological evaluation of compounds isolated from *Curculigo orchioides*. There are a few studies evaluating the activities of extracts from this plant,

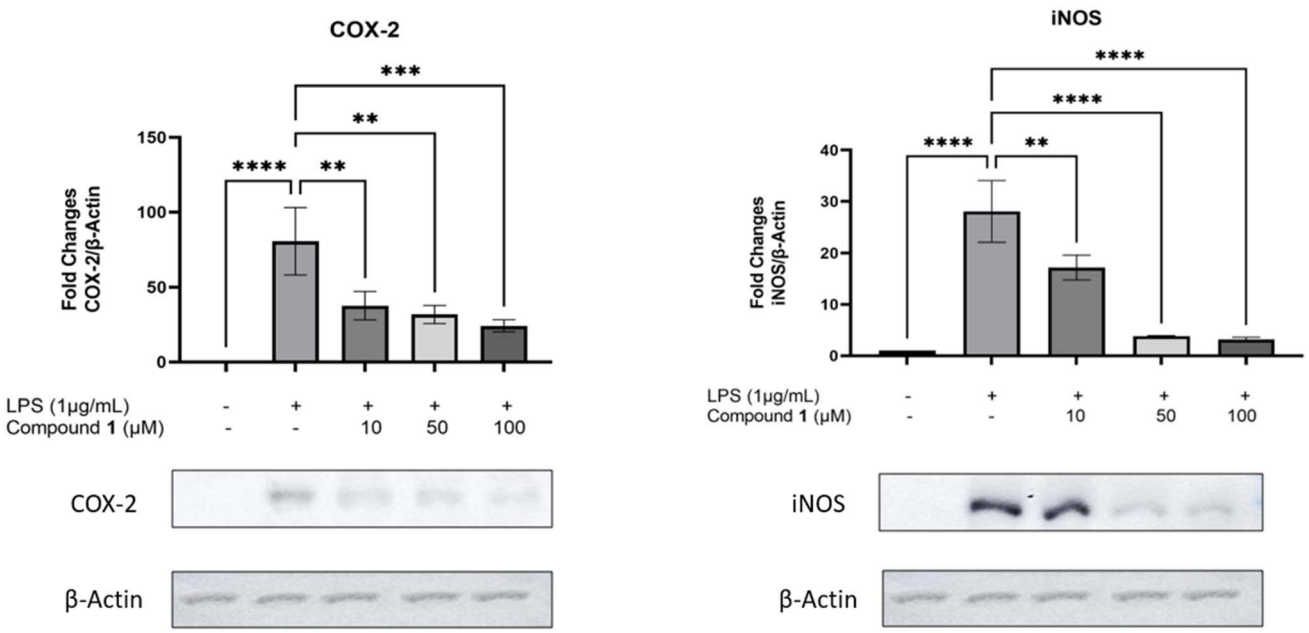

Fig. 4 Effect of compound **1** on the expression of iNOS, COX-2, and β-actin in LPS-stimulated RAW 264.7 cells. Cells were pre-treated with three concentrations around the IC_{50} value of compound **1** (10, 50, and 100 μM) for 30 minutes, followed by stimulation with LPS (1 μg mL^{-1}) for 24 hours. Total cells were harvested for the western blotting experiment. An immunoblot was performed with anti-iNOS, anti-COX2, and anti-β-actin primary antibodies. Images were captured by ImageQuant LAS 500. The data are expressed as mean ± SD ($n = 3$; **$p < 0.01$; ****$p <$ 0.0001, compared to LPS-treated controls).

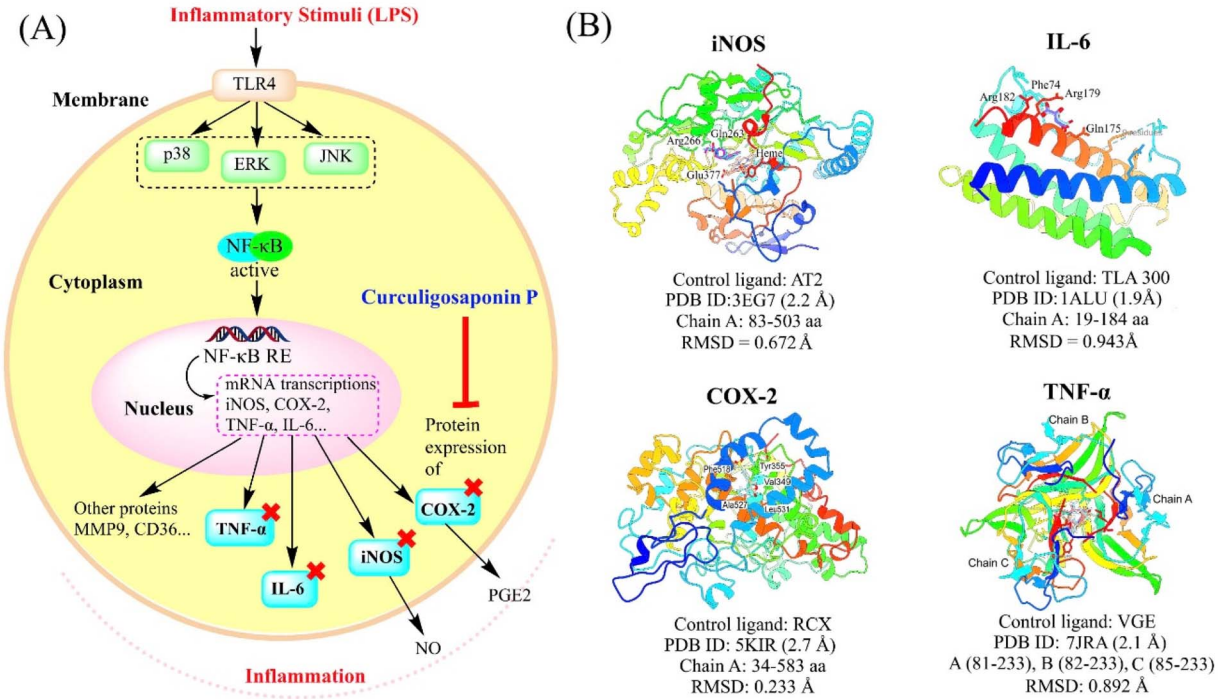

Fig. 5 Molecular pathway and structure analysis of compound **1**. (A) A diagram of the proposed anti-inflammatory mechanism of compound **1** on RAW 264.7 cells. (B) Redocking results of cocrystal ligands in the active sites of for enzymes (iNOS, IL-6, TNF-α, and COX-2) together with their structural information.

including anti-inflammatory and antioxidant activities,[10] however, the main active compounds and their underlying mechanisms of action have not been fully investigated. Our study is the first to isolate six new compounds from *C. orchioides* and evaluate their anti-inflammatory activities *in vitro* on the RAW 264.7 macrophage model. This makes an important contribution to the phytochemical and pharmacological profiling of this traditionally used medicinal plant.

Molecular docking analysis of the compound 1

According to the biological evaluation, pure compounds isolated from *Curculigo orchioides* exhibited anti-inflammatory activities on RAW 264.7 cells, especially compound **1**. We therefore propose that compound **1** exerts anti-inflammatory activity on RAW 264.7 cells by inhibiting NO, PGE2, TNF-α, and IL-6 production in macrophages. To confirm our hypothesis, we performed docking studies of compound **1** with four targets, including iNOS, IL-6, TNF-α, and COX-2, following the methods previously reported.[16] Since the other 4 compounds, such as **2**, **3**, **4**, and **6**, showed inhibitory activity in the iNOS assay, all the natural compounds were also simulated to compare their interactions with this enzyme.

The docking protocol was first validated by removing and redocking the co-crystallized ligands into the active sites of the target proteins. The resulting redocked conformations exhibited strong alignment with the original ligand poses, with RMSD values ranging from 0.233 to 0.943 Å (Fig. 5B). Importantly, key interactions between the co-crystal ligands and their respective targets were well preserved. For example, the aminopyridine co-crystal inhibitor demonstrated selective binding to iNOS through electrostatic and hydrophobic interactions within the heme pocket of the active site. Its parallel stacking over the heme plane, referred to as anchored plasticity, was crucial for this selectivity (Fig. 6A). According to Garcin *et al.*, selective inhibition also involves hydrogen bonding with Glu377 and interactions with a network of residues forming the second and third-shell layers above the heme cofactor.[11] The binding energy calculated for this cocrystal ligand was −8.19 kcal mol^{-1}. These redocking results confirm the reliability and validity of the docking protocol applied to iNOS. Likewise, the redocking outcomes for IL-6, TNF-α, and COX-2 were also consistent and accurate. Notably, the redocked conformer of the TNF-α co-crystal antagonist exhibited a close overlap with the original ligand (RMSD = 0.892 Å) and maintained key interactions within the hydrophobic core formed by chains A, B, and C of the trimeric cytokine TNF-α.[13] In case of COX-2, the redocked conformer of rofecoxib closely aligned with its co-crystal structure, showing a low RMSD of 0.233 Å. Rofecoxib demonstrates selective inhibition of COX-2 through multiple stacking interactions within the hydrophobic cavity adjacent to the heme prosthetic group, involving key residues such as Phe381, Leu483, Tyr385, Trp387, and Gly526.[29] The binding energies, calculated using a two-step scoring approach (London dG and GBVI/WSA dG), were −8.633, −9.132, and −8.283 kcal mol^{-1} for IL-6, TNF-α, and COX-2, respectively.

The next step involved evaluating the binding affinity of the natural compounds, particularly compound **1**, against four proteins iNOS, IL-6, TNF-α, and COX-2, using the previously

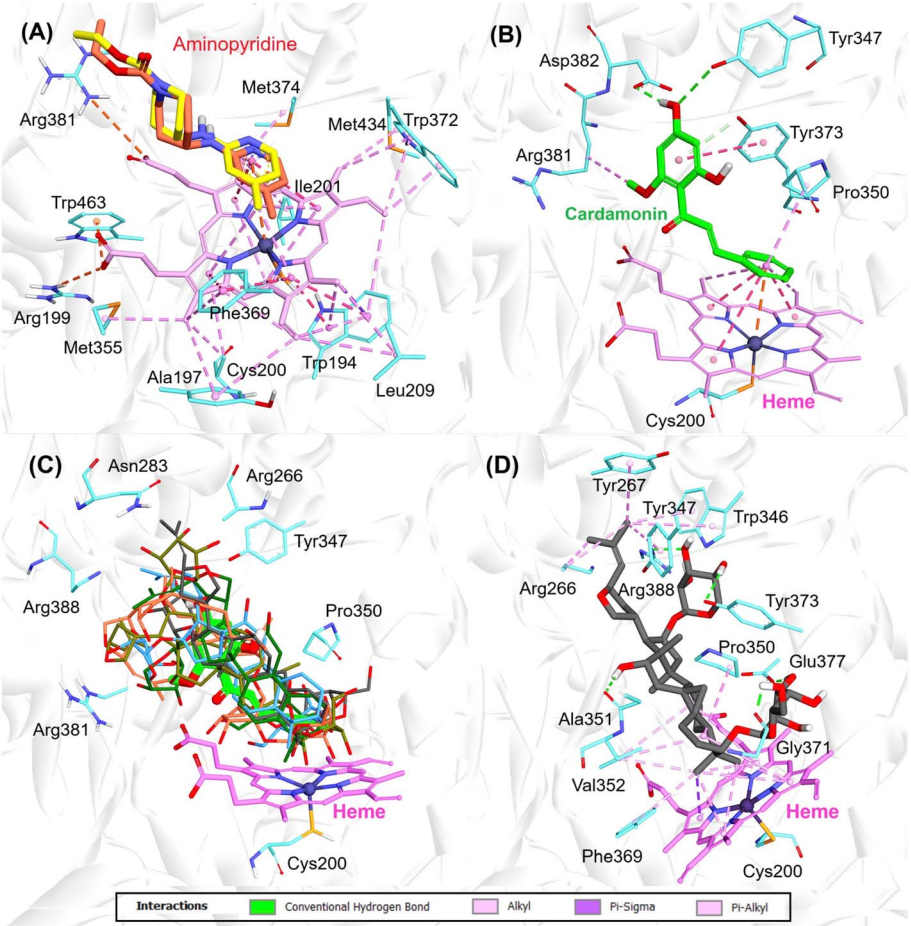

Fig. 6 Interactions of the docked compounds in the active site of iNOS. (A) Superposition of cocrystal aminopyridine inhibitor, (B) positive control cardamonin, (C) orientation of five natural compounds (colored by C-chains) highly overlapped with cardamonin, (D) 3D interactions of compound **1**.

validated docking protocol. We first focused on iNOS, comparing the docking results of all five natural compounds with the positive control, cardamonin (Fig. 6). Cardamonin demonstrated notable selectivity through interactions between its electrophilic benzene ring and Fe(II), along with multiple π–π stacking interactions with the heme plane (interplanar angle ~ 20°). All five natural compounds also exhibited stacking interactions with the pyrrole rings of the heme group; however, they lacked coordination with Fe(II), and the stacking interactions were primarily π–alkyl, which are generally 2- to 3-fold weaker than the π–aryl interactions observed in cardamonin.[30] The strength of stacking interactions followed the order: compound **1** > **2** > **6** > **4** > **3**, aligning with experimental observations. Notably, compound **1** also engaged in key hydrogen bonds with Glu377 and formed interactions across all three distant residue shells, consistent with the anchored plasticity mechanism described by Garcin *et al.*[11] In addition, the binding energy of compound **1** was −7.91 kcal mol^{-1}, slightly lower than that of cardamonin. These findings indicate that compound **1** is a promising hit compound with anti-inflammatory activity through selective inhibition of iNOS.

Focusing on compound **1**, we further conducted docking simulations with IL-6, TNF-α, and COX-2. Fig. 7 summarizes the binding poses and molecular interactions of compound **1** within the active sites of these targets. Of note, compound **1** appears capable of disrupting the interaction between IL-6 and its receptor by engaging key hotspot residues, Leu33, Gln175, and Arg179, similar to the native cocrystal ligand.[12,31] Additionally, its glycoside moiety formed hydrogen bonds with adjacent residues near the binding site, including Asp34 and Ser37, potentially enhancing its binding stability and specificity. Its binding energy was −8.1 kcal mol^{-1}. For TNF-α, compound **1** was found to penetrate deeply into the binding cavity formed at the interface of chains A, B, and C. It established multiple π-stacking interactions with key residues, including Tyr135C, Leu133A–B, Ile231A–C, and Leu233A–C, as well as with a small hydrophobic pocket formed by the side chains of Tyr195B–C (Fig. 7B). These interactions are consistent with previously reported findings, which highlight the importance of engaging these residues for effective TNF-α inhibition.[13]

The calculated binding energy for compound **1** was −7.69 kcal mol^{-1}, significantly lower than that of the cocrystal

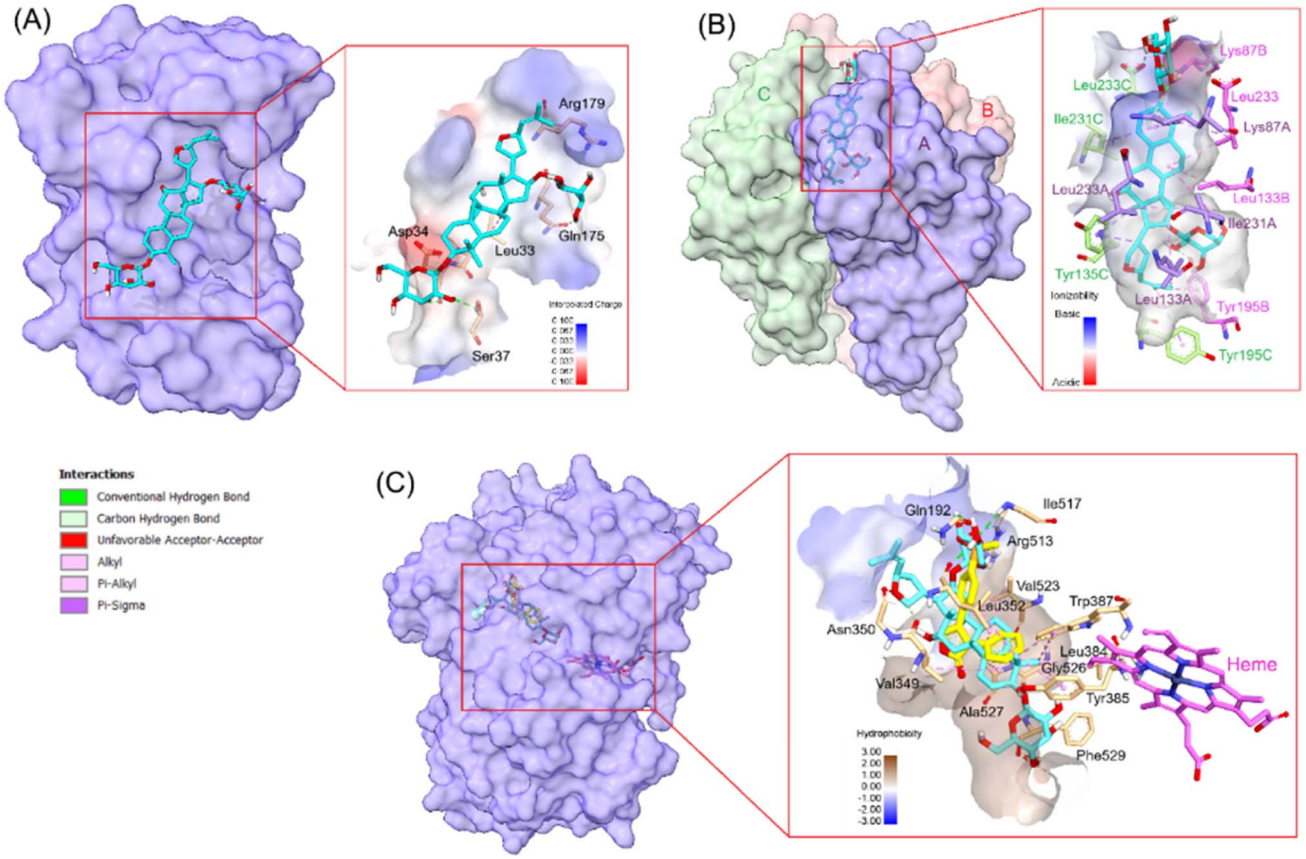

Fig. 7 Docking results and interactions of compound **1** (cyan carbon) in the binding sites of IL-6, TNF-α, and COX-2. (A) IL-6 (PDB ID: 1ALU),[12] (B) TNF-α (PDB ID: 7JRA),[13] and (C) COX-2 (PDB ID: 5KIR).[14]

inhibitor. Finally, docking studies were performed on the COX-2 enzyme, and the interactions of compound **1** were compared with those of the selective inhibitor rofecoxib. In our recent work, we emphasized the critical role of stacking interactions within the narrow channel located inside the catalytic domain of COX-2.[29] As illustrated in Fig. 7C, the triterpene backbone linked to a glycoside moiety was able to insert effectively into this hydrophobic lobby cavity, forming multiple π–alkyl stacking interactions with key residues, including Val349, Tyr385, Tyr387, Val523, and Ala527. These residues, which constitute part of the α-helix adjacent to the heme group, are known to contribute to COX-2's oxygenase activation. However, two unfavorable acceptor–acceptor interactions were observed with Phe529 and Asn350, particularly near the entrance of the binding pocket. These interactions may hinder optimal ligand stabilization within the active site. The binding energy of compound **1** was calculated to be −7.01 kcal mol^{-1}, which is moderately lower than that of rofecoxib (−8.283 kcal mol^{-1}).

Conclusions

Six novel cycloartane-type saponins were isolated from *Curculigo orchioides*, among which compound **1** (curculigosaponin P) exhibited anti-inflammatory activity by inhibiting the production of NO, TNF-α, and IL-6, and downregulating iNOS and COX-2 expression. Molecular docking further showed that compound **1** interacts favorably with key inflammatory targets iNOS, IL-6, TNF-α, and COX-2, supporting its observed bioactivity. To the best of our knowledge, this is the first study reporting the isolation and anti-inflammatory evaluation of these compounds from *Curculigo orchioides*.

Conflicts of interest

The authors declare no competing financial interests.

Data availability

The data that support the findings of this study are available from the corresponding author upon reasonable request. Supplementary information is available. See DOI: **https://doi.org/10.1039/d5ra04849d**.

Acknowledgements

The authors are grateful to the University of Science and Technology of Hanoi (USTH) for financial support under the grant for Top-tier Research Group Phytomed.

References

1 R. Medzhitov, *Nature*, 2008, **454**, 428–435.
2 H. E. Vonkeman and M. A. F. J. van de Laar, *Semin. Arthritis Rheum.*, 2010, **39**, 294–312.
3 D. J. Newman and G. M. Cragg, *J. Nat. Prod.*, 2020, **83**, 770–803.
4 Y. Nie, X. Dong, Y. He, T. Yuan, T. Han, K. Rahman, L. Qin and Q. Zhang, *J. Ethnopharmacol.*, 2013, **147**, 547–563.
5 A. R. Bafna and S. H. Mishra, *J. Ethnopharmacol.*, 2006, **104**, 1–4.
6 W.-L. Chang, M.-J. Su and S.-S. Lee, *J. Nat. Prod.*, 1997, **60**, 76–80.
7 A. Yokosuka, K. Sato and Y. Mimaki, *Phytochemistry*, 2010, **71**, 2174–2181.
8 A. Yokosuka, K. Sato, T. Yamori and Y. Mimaki, *J. Nat. Prod.*, 2010, **73**, 1102–1106.
9 Q. Wu, D.-X. Fu, A.-J. Hou, G.-Q. Lei, Z.-J. Liu, J.-K. Chen and T.-S. Zhou, *Chem. Pharm. Bull.*, 2005, **53**, 1065–1067.
10 V. Lakshmi, K. Pandey, A. Puri, R. P. Saxena and K. C. Saxena, *J. Ethnopharmacol.*, 2003, **89**, 181–184.
11 E. D. Garcin, A. S. Arvai, R. J. Rosenfeld, M. D. Kroeger, B. R. Crane, G. Andersson, G. Andrews, P. J. Hamley, P. R. Mallinder, D. J. Nicholls, S. A. St-Gallay, A. C. Tinker, N. P. Gensmantel, A. Mete, D. R. Cheshire, S. Connolly, D. J. Stuehr, A. Aberg, A. V Wallace, J. A. Tainer and E. D. Getzoff, *Nat. Chem. Biol.*, 2008, **4**, 700–707.
12 W. Somers, M. Stahl and J. S. Seehra, *EMBO J.*, 1997, **16**, 989–997.
13 H.-Y. Xiao, N. Li, J. J.-W. Duan, B. Jiang, Z. Lu, K. Ngu, J. Tino, L. M. Kopcho, H. Lu, J. Chen, A. J. Tebben, S. Sheriff, C. Y. Chang, J. J. Yanchunas, D. Calambur, M. Gao, D. J. Shuster, V. Susulic, J. H. Xie, V. R. Guarino, D.-R. Wu, K. R. Gregor, C. B. Goldstine, J. J. Hynes, J. E. Macor, L. Salter-Cid, J. R. Burke, P. J. Shaw and T. G. M. Dhar, *J. Med. Chem.*, 2020, **63**, 15050–15071.
14 B. J. Orlando and M. G. Malkowski, *Acta Crystallogr., Sect. F: Struct. Biol. Commun.*, 2016, **72**, 772–776.
15 M. S. Ummah, *Molecular Operating Environment (MOE), version 2015.10*, Chemical Computing Group ULC, Montreal, QC, Canada, 2015, pp. 910–1010.
16 T. T. Phuong Tran, N. X. Nhiem, H. Pham-The, U. T. T. Phan, L. T. Huong and H. D. Nguyen, *Chem. Biodiversity*, 2024, **21**, e202401224.
17 T. T. Lan, D. T. Anh, P.-T. Hai, D. T. M. Dung, L. T. T. Huong, E. J. Park, H. W. Jeon, J. S. Kang, N. T. Thuan, S.-B. Han and N.-H. Nam, *Med. Chem. Res.*, 2020, **29**, 396–408.
18 D. Ramírez and J. Caballero, *Molecules*, 2018, **23**, 1038.
19 E. F. Pettersen, T. D. Goddard, C. C. Huang, E. C. Meng, G. S. Couch, T. I. Croll, J. H. Morris and T. E. Ferrin, *Protein Sci.*, 2021, **30**, 70–82.
20 H. Otsuka, J. Shitamoto, D.-H. He, K. Matsunami, T. Shinzato, M. Aramoto, Y. Takeda and T. Kanchanapoom, *Chem. Pharm. Bull.*, 2007, **55**, 1600–1605.
21 J. Kitajima, C. Okamura, T. Ishikawa and Y. Tanaka, *Chem. Pharm. Bull.*, 1998, **46**, 1595–1598.
22 M. Kubo, H. Sasaki, T. Endo, H. Taguchi and I. Yoshioka, *Chem. Pharm. Bull.*, 1986, **34**, 3097–3101.
23 H. Achenbach and D. Frey, *Phytochemistry*, 1992, **31**, 4263–4274.
24 M. Park, D. Ryu, J. Cho and K. Ku, *Molecules*, 2024, **29**, 403.
25 H. M. Abdallah, F. M. Almowallad, A. Esmat, I. A. Shehata and E. A. Abdel-Sattar, *Phytochem. Lett.*, 2015, **13**, 74–80.
26 C. T. Yen, C. L. Lee, F. R. Chang, T. L. Hwang, H. F. Yen, C. J. Chen, S. L. Chen and Y. C. Wu, *J. Nat. Prod.*, 2012, **75**, 636–643.
27 L. T. Huong, P. A. Thu, P. T. Dao, D. T. M. Huong, P. V. Cuong and N. H. Dang, *Chem. Biodiversity*, 2021, **18**, e2100518.
28 M. S. Choi, S. H. Lee, H. S. Cho, Y. Kim, Y. P. Yun, H. Y. Jung, J. K. Jung, B. C. Lee, H. B. Pyo and J. T. Hong, *Eur. J. Pharmacol.*, 2007, **556**, 181–189.
29 T. Solongo, T. T. Huong, E. Purevdorj, A. Solongo, B. Bayasgalan, V. T. Loc, N. X. Ha, V. T. Ha, N. P. Hung, D. T. Thao, N. T. Nga, H. P. - The, P. Stark and N. M. Cuong, *J. Nat. Med.*, 2025, **79**, DOI: **10.1007/s11418-025-01882-x**.
30 J. Ribas, E. Cubero, F. J. Luque and M. Orozco, *J. Org. Chem.*, 2002, **67**, 7057–7065.
31 H. T. Nguyen, H. Pham-The, A. N. Tuan, H. N. T. Thu, T. A. D. Thi, G. Le-Nhat-Thuy, P. H. Thi, Q. G. N. Thi and T. Van Nguyen, *Bioorg. Med. Chem. Lett.*, 2024, **104**, 129714.